JACS
JOURNAL OF THE AMERICAN CHEMICAL SOCIETY

Article

pubs.acs.org/JACS

Synthesis and Controlled Self-Assembly of Covalently Linked Hexa-*peri*-hexabenzocoronene/Perylene Diimide Dyads as Models To Study Fundamental Energy and Electron Transfer Processes

Lukas F. Dössel,[†] Valentin Kamm, Ian A. Howard, Frédéric Laquai, Wojciech Pisula,[†] Xinliang Feng, Chen Li, Masayoshi Takase,[§] Tibor Kudernac,[‡] Steven De Feyter,[‡] and Klaus Müllen*

Max Planck Institute for Polymer Research, Ackermannweg 10, D-55128 Mainz, Germany

Supporting Information

ABSTRACT: We report the synthesis and photophysical characterization of a series of hexa-*peri*-hexabenzocoronene (HBC)/perylenetetracarboxy diimide (PDI) dyads that are covalently linked with a rigid bridge. Both the ratio of the two components and the conjugation of the bridging element are systematically modified to study the influence on self-assembly and energy and electron transfer between electron donor HBC and acceptor PDI. STM and 2D-WAXS experiments reveal that both in solution and in bulk solid state the dyads assemble into well-ordered two-dimensional supramolecular structures with controllable mutual orientations and distances between donor and acceptor at a nanoscopic scale. Depending on the symmetry of the dyads, either columns with nanosegregated stacks of HBC and PDI or interdigitating networks with alternating HBC and PDI moieties are observed. UV−vis, photoluminescence, transient photoluminescence, and transient absorption spectroscopy confirm that after photoexcitation of the donor HBC a photoinduced electron transfer between HBC and PDI can only compete with the dominant Förster resonance energy transfer, if facilitated by an intimate stacking of HBC and PDI with sufficient orbital overlap. However, while the alternating stacks allow efficient electron transfer, only the nanosegregated stacks provide charge transport channels in bulk state that are a prerequisite for application as active components in thin film electronic devices. These results have important implications for the further design of functional donor−acceptor dyads, being promising materials for organic bulk heterojunction solar cells and field-effect transistors.

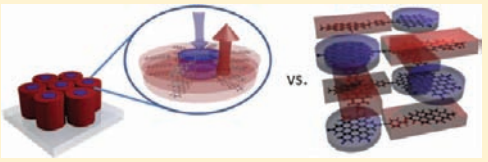

INTRODUCTION

In the emerging field of organic opto-electronics, control of the supramolecular organization within the active layer has been found to be a key factor affecting the properties and the performance of thin film devices.[1−8] Especially when blends of self-organizing donor and acceptor moieties are utilized, their mutual orientation and the degree of supramolecular ordering are of importance in controlling the fundamental energy and electron transfer processes and the existence of continuous percolation pathways for charge carriers.[9−13] For this reason, small discotic molecules such as hexa-*peri*-hexabenzocoronene (HBC) and perylenetetracarboxy diimide (PDI) were found to be promising candidates, as they can be functionalized to self-assemble into columnar superstructures in bulk state with a pronounced phase separation on the nanometer scale, creating efficient transport channels for charge carriers while maintaining very thorough donor−acceptor mixing.[14,15] Electron-donating (D) HBC exhibits the highest charge carrier mobility of all discotic liquid crystals,[16,17] while the crystalline acceptor (A) PDI possesses a high electron mobility[18,19] and excellent chemical, thermal, photochemical, and photophysical stability.[20,21] Based on a fast intermolecular photoinduced electron transfer at the donor−acceptor interface, blends of HBC and PDI have been successfully used to build photovoltaic devices with remarkably high external quantum efficiencies by simple solution processing.[15,22,23] The excellent performance is mainly attributed to the horizontal phase separation within the active layer, providing a large interfacial area and close packing between D and A domains. However, at present these blends lack any means of control of the supramolecular ordering and phase separation at the nanometer scale, leading to defects that promote charge trapping, charge recombination, and competing processes such as Förster type energy transfer within the active layer.

In contrast, controlled phase separation at this desired scale can be introduced by chemical design of organic semiconducting molecules. Covalent linkage in D−A dyads can offer full control over the self-organization and orientation of the molecular units to one another.[2,24] Furthermore, by using a rigid bridge, the distance between D and A can be set within the nanoscopic dimension to optimize charge carrier mobilities and achieve fast exciton dissociation to suppress energy transfer processes. Such dyads incorporating HBC and perylene derivatives have recently been synthesized, and their self-assembly and electronic properties have been investigated.[2,25,26] Highly ordered and nanosegregated π-stacks were found to exhibit an ambipolar behavior in a field-effect transistor device with high charge carrier mobilities.[2] To further broaden the scope of potential applications for such dyads, a detailed

Received: December 8, 2011
Published: March 6, 2012

   dx.doi.org/10.1021/ja211504a | *J. Am. Chem. Soc.* 2012, 134, 5876−5886

Scheme 1. Chemical Formulas of the HBC-PDI Dyads 1−5

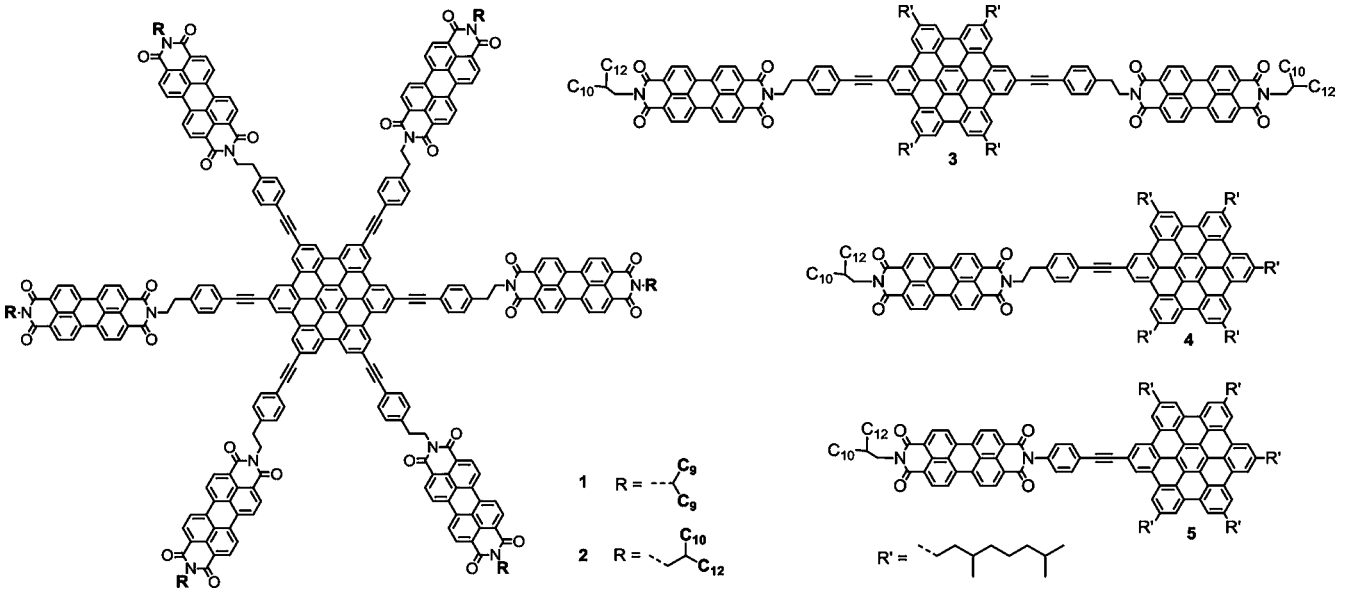

Scheme 2. Synthesis of the Asymmetric PDI Building Blocks 10a, 10b, and 15[α]

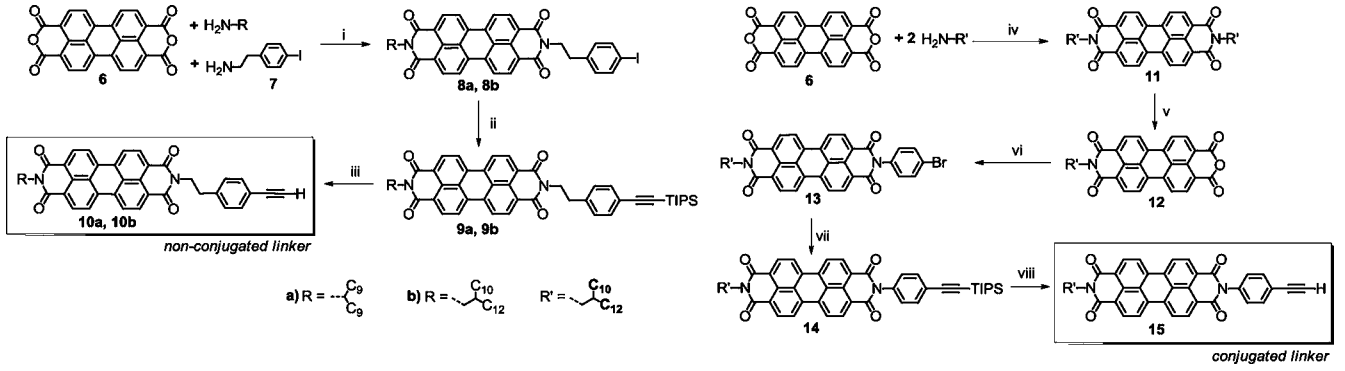

[α]Reagents and conditions: (i) *N*-methyl-2-pyrrolidone (NMP), HCl, 130 °C, 34% (a), 26% (b); (ii) TIPS-acetylene, $Pd(PPh_3)_4$, CuI, tetrahydrofuran, Et_3N, 70 °C, 83% (a), 73% (b); (iii) TBAF, tetrahydrofuran, rt, 95% (a), 97% (b); (iv, v) synthesized according to literature;[27,28] (vi) *p*-bromoaniline, propanoic acid, 54%; (vii) TIPS-acetylene, $Pd(PPh_3)_4$, CuI, piperidine, 70 °C, 67%; (vii) TBAF, tetrahydrofuran, rt, 99%.

understanding of the interactions between donor and acceptor moieties, the resulting supramolecular organization, and its effect on the fundamental photophysical processes is required. In this study, we investigated whether HBC-PDI dyads can be designed to self-assemble into well-defined supramolecular structures with tailored energy and charge transfer processes after photoexcitation.

Herein, we present a series of novel HBC-PDI dyads **1**−**5** (Scheme 1) with rigid covalent linkers that were fully characterized regarding their fundamental interactions between donor and acceptor moieties. Driven by noncovalent intermolecular interactions, the dyads assembled into well-ordered two-dimensional structures with controllable mutual orientations and distances between D and A at a nanoscopic scale, both in solution and in the solid state. As the pronounced π-stacking tendencies of both HBC and PDI are known to reduce solubility, limit purification, and hamper analytical methods, sterically demanding alkyl chains were introduced in the periphery of the dyads **1**−**5**. After self-assembly, the donor moiety was selectively excited to study intramolecular and intermolecular decay channels of the generated excitons. To promote a fast intramolecular charge transfer, a fully conjugated *p*-phenyleneethynylene linker was used in dyad **5**, whereas for **1**−**4** an additional nonconjugated ethylene unit was introduced to inhibit direct charge recombination. The ethynylene bridging had the advantage of allowing a Sonogashira coupling that promised high yields, fewer side products, and reduced steric hindrance in comparison to a single bond.[2] The rigidity of the linker was required to prevent intramolecular formation of a charge-transfer (CT) complex between D and A. Both in bulk and in solution intermolecular D−A interactions were found to be the dominant forces for phase separation and self-organization, leading to alternating stacks of HBC and PDI, unless inhibited by a nonstoichiometric ratio that resulted in strictly segregated columns. Depending on the type of supramolecular ordering, either an efficient intermolecular electron transfer was observed for alternating stacks or a fast intramolecular energy transfer for segregated stacking, with the latter preserving potential percolation pathways for both holes and electrons (ambipolar transport). Scanning tunneling microscopy (STM) of physisorbed aggregates and the solvent−HOPG interface was utilized to study self-assembly in solution and interactions with the graphite surface, while bulk samples were analyzed by two-dimensional wide-angle X-

dx.doi.org/10.1021/ja211504a | J. Am. Chem. Soc. 2012, 134, 5876−5886

Scheme 3. Synthesis of the HBC-PDI Dyads 1−5 via Sonogashira−Hagihara Cross-Coupling Reaction[α]

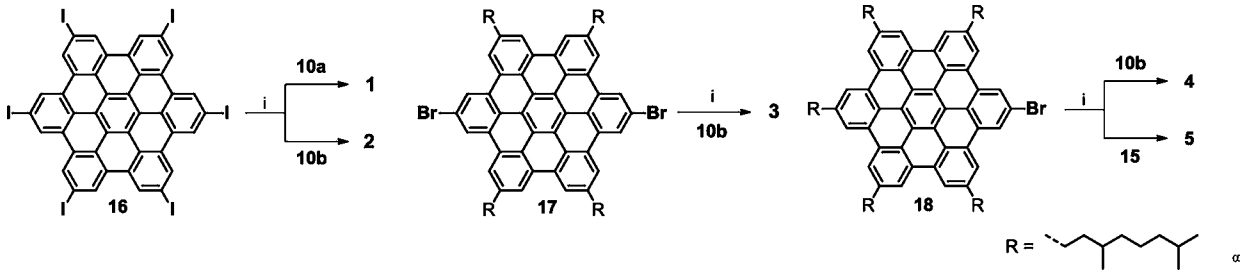

[α]Reagents and conditions: (i) $Pd(PPh_3)_4$, CuI, piperidine/tetrahydrofuran, 80 °C, 51% (**1**), 31% (**2**), 10% (**3**), 86% (**4**), 5% (**5**).

ray scattering (2D-WAXS) in extruded filaments. Photophysical processes after photoexcitation were investigated in solution and in thin films by UV−vis, steady state, and transient photoluminescence (PL) spectroscopy.

RESULTS AND DISCUSSION

Synthesis. Dyads **1**−**5** were synthesized according to the synthetic procedure depicted in Schemes 1 and 2. A palladium-catalyzed Sonogashira cross-coupling reaction of an ethynyl-PDI (**10a**, **10b**, or **15**) with a halogenated HBC moiety was utilized in the final reaction step. This was in contrast to previously reported dyads of HBC and PDI, where an ethynyl-HBC and a halogenated PDI were coupled. As potential Glaser-type cross-linking reactions of 2-fold or 6-fold ethynyl-functionalized HBCs would dramatically reduce the yields, this was avoided by introducing the ethynyl function to the PDI. Synthesis of the asymmetric PDI compounds **10a** and **10b** could be achieved by a statistic imidization of commercial perylenetetracarboxy dianhydride **6** with 2 equiv of 4-bromophenethylamine **7** and 10-nonadecylamine (**8a**) and 2-decyl-tetradecylamine (**8b**), respectively, which had to be synthesized following known literature procedures.[29−31] Due to the limited solubility of the starting material, the reaction had to be conducted at 130 °C, to finally yield 26−34% of PDIs **8a**/**b** after purification via column chromatography on silica gel as red waxy solids. The iodo function now allowed the introduction of a triisopropylsilyl-protected (TIPS) ethynyl function via Sonogashira coupling reaction ($Pd(PPh_3)_4$, CuI, piperidine) to give **9a**/**b** in high yields (73−83%). Subsequent desilylation with tetra-*n*-butylammonium fluoride (TBAF) gave the final PDIs **10a** and **10b** with a nonconjugated ethylene linker and an unprotected ethynyl function in almost quantitative yields (95−97%) as red solids. To prevent oxygen-promoted Glaser homocoupling during storage, the compounds were kept refrigerated under argon atmosphere.

Attempts to also obtain the asymmetric PDI **13** (Scheme 2) with a fully conjugated linker via statistical imidization did not yield any product. Due to a limited reactivity of the aromatic *p*-bromoaniline in comparison to aliphatic primary amines, only a 2-fold reaction of the 2-decyl-tetradecylamine was observed. So a more complex literature-known synthetic route had to be used, employing the selective alkaline hydrolysis of the symmetric PDI **11** to obtain the perylene monoimide-monoanhydride **12**.[27,28] Under harsh reaction conditions (160 °C, 6 d) and use of 5 equiv of *p*-bromoaniline the asymmetric PDI **13** could be obtained in 54% yield after column chromatographic purification. Despite the presence of a sterically demanding alkyl chain in the periphery, **13** showed only limited solubility in common organic solvents like tetrahydrofuran, toluene or dichloromethane, due to the rigidity of the rest of the molecule. This hampered purification and spectroscopic characterization. Subsequent Sonogashira coupling reaction ($Pd(PPh_3)_4$, CuI, piperidine) with TIPS-acetylene was used to introduce the ethynyl group in PDI **14** with 67% yield, resulting in a dramatic increase in solubility. Finally the TIPS protecting group was cleaved off with TBAF at room temperature to obtain PDI **15** with a free ethynyl function. Despite the reduced solubility, column chromatography quantitatively yielded PDI **15** as a red solid (99%). All PDI compounds (**10a**/**b** and **15**) could be characterized by field desorption (FD) mass spectrometry, NMR spectroscopy, and elemental analysis.

In a final reaction step, the PDI compounds were covalently connected to the corresponding HBC core via Sonogashira cross-coupling (Scheme 3). To avoid homocoupling of the alkyne compounds, the reaction mixtures were thoroughly degassed by several "freeze−pump−thaw" cycles, before the catalysts were added. For the star-shaped HBC-6PDI compounds **1** and **2** a 6-fold functionalized hexakis(4-iodo)-hexa-*peri*-hexabenzocoronene **16** was used, which had been synthesized following a known literature procedure.[32] As the HBC compound **16** exhibited very poor solubility, the reaction had to be conducted in a solvent mixture of piperidine and tetrahydrofuran at 70−80 °C overnight. At the same time, 12 equiv of PDIs **10a**/**10b** had to be used in order to reduce the amount of incompletely substituted side products. Even though the reaction conditions were carefully optimized, matrix-assisted laser desorption/ionization time-of-flight (MALDI-TOF) MS detected 5-fold substituted side products that could not be separated using recrystallization or column chromatography. At this point, recycling preparative gel permeation chromatography (GPC) was employed to isolate the desired HBC-6PDI dyads **1** and **2** with maximum purity. After workup, both target compounds could be obtained as red solids with yields of 51% and 31%, respectively. Originating from strong intermolecular $\pi-\pi$ interactions, both samples showed very limited solubility in common organic solvents, which hampered analysis by NMR spectroscopy. In conformity with previous reports in the literature, satisfactory elemental analysis results could not be obtained, possibly due to incomplete combustion and soot formation of the extended aromatic cores.[33] However, MALDI-TOF MS (Figure 1) and high resolution STM experiments were able to verify the structure and the purity of HBC-6PDI dyads **1** and **2**.

Following the same synthetic procedure toward HBC-2PDI **3**, 3 equiv of PDI **10b** was reacted with the 2-fold halogen-functionalized 1,10-dibromo-4,7,13,16-tetra(3,7-dimethyl-octyl)-hexa-*peri*-hexabenzocoronene **17** (Scheme 3), which

dx.doi.org/10.1021/ja211504a | J. Am. Chem. Soc. 2012, 134, 5876−5886

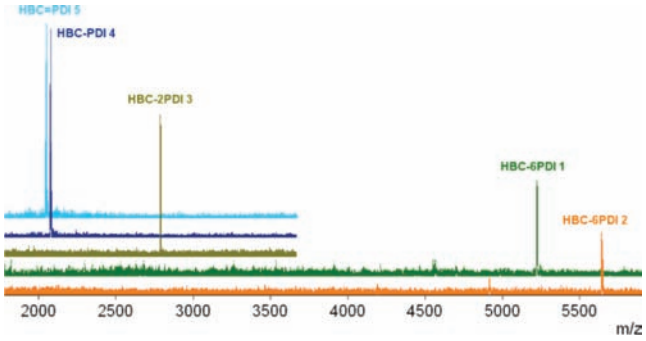

Figure 1. MALDI-TOF MS of dyads **1**–**5** after purification via recycling GPC, proving full removal of incompletely substituted side products. For details see Experimental Section.

had been prepared according to literature.[34] To increase solubility, vacant positions on the HBC were decorated with four branched 3,7-dimethyloctyl alkyl chains. Due to a lowered reactivity of the bromo as compared to the iodo function, a complete 2-fold substitution could not be achieved either by applying more drastic reaction conditions or by using a larger excess of PDI **10b**. Finally, the raw product mixture was purified by column chromatography and subjected to another Sonogashira coupling reaction with 2 equiv of PDI **10b** and fresh catalysts to increase the amount of HBC-2PDI **3** in the reaction mixture. After purification utilizing the recycling GPC technique, dyad HBC-2PDI **3** could be isolated in 10% yield as a dark red solid that showed limited solubility, solely allowing for analysis with MALDI-TOF MS (Figure 1).

To synthesize HBC-1PDI **4**, 1-bromo-4,7,10,13,16-penta-(3,7-dimethyl-octyl)-hexa-*peri*-hexabenzocoronene **18**[34] was coupled with an excess of PDI **10b**, following the same synthetic protocol as the other dyads (Scheme 3). Dyad HBC-1PDI **4** exhibited excellent solubility in common organic solvents and allowed for easy purification with recycling GPC, yielding 86% of a dark red solid. MALDI-TOF MS, elemental analysis, ^{1}H NMR spectroscopy, and two-dimensional H–H NOESY NMR experiments confirmed the structure and purity of the molecule. For the directly conjugated HBC=1PDI **5**, 1.5 equiv of PDI **15** was reacted with HBC **18**. Due to the pronounced rigidity, the resulting dyad **5** showed strong self-aggregation tendency and low solubility, even at low concentrations. Finally repetitive usage of the recycling GPC system allowed isolation of dyad HBC=1PDI **5**, yielding 10% of a dark red solid. In addition to MALDI-TOF MS (Figure 1), the product could also be characterized by ^{1}H NMR spectroscopy at elevated temperatures.

In Figure 1, the relevant sections of the superimposed MALDI-TOF MS of dyads **1**–**5** are presented, showing the compounds after recycling GPC purification and proving full removal of incompletely substituted side products. The HBC-6PDIs **1** and **2** with molecular weights of more than 5000 g/mol required a solvent-free sample preparation[35,36] and increased laser power to create a sufficient signal-to-noise ratio. Under these conditions fragmentation occurred, which correlated with the excitation energy and could no longer be observed at low laser powers.

Self-Assembly in Solution (NMR). A characteristic feature of HBC and PDI is their tendency to aggregate in a face-to-face fashion in the solid state as well as in solutions. Aggregation of HBC has been observed even at concentrations as low as 10^{-9} mol/L.[37] Because of the pronounced intermolecular π–π interactions, ^{1}H NMR experiments of dyads HBC-1PDI **4** and HBC=1PDI **5** in dilute solutions and at elevated temperatures still revealed a pronounced upfield shift of the aromatic proton resonances. PDI proton signals were even shifted by more than 1.5 ppm in comparison to the isolated PDI building blocks **10a** and **10b** (see Supporting Information). This effect was caused by additional intermolecular donor–acceptor interactions within aggregates.[38,39] For the star-shaped HBC-6PDIs **1** and **2** that carry multiple chromophores, a more pronounced aggregate formation was observed, leading to strong broadening of the signals in NMR experiments and no distinct effect of concentration or temperature, suggesting the formation of stable aggregates. Here, STM experiments at the liquid–solid interface were utilized to image dyads **1** and **2** after adsorption on Au(111) substrates.

Self-Assembly at the Solid–Liquid Interface (STM). STM imaging of the HBC-6PDIs **1** and **2** after physisorption of submonolayers onto Au(111) surfaces from dilute solutions in 1-phenyloctane and 1,2,4-trichlorobenzene allowed imaging of the molecules with molecular resolution. Independent of the solvent used, both dyads showed a strong tendency to form dimer-like structures where both HBC and PDI were adsorbed on the gold surface in a staggered conformation (face-to-face). In the STM height images (Figure 2a–c), the circular structure

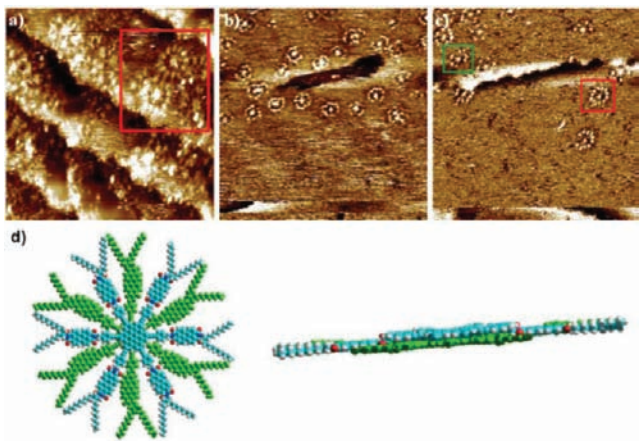

Figure 2. STM height images of HBC-6PDIs **1** and **2** in submonolayers at the liquid–solid interface using 1-phenyloctane and 1,2,4-trichlorobenzene (TCB) as the solvents. Some dimer-type aggregates are highlighted with red boxes, a single dyad with a green box. (a) **2**, phenyloctane/Au(111), 39.0 × 39.0 nm^2, I_{set} =100 pA, V_{bias} = 560 mV; (b) **2**, TCB/Au(111), 69.7 × 69.7 nm^2, I_{set} = 80 pA, V_{bias} = 423 mV; (c) **1**, TCB/Au(111), 107.2 × 107.2 nm^2, I_{set} = 109 pA, V_{bias} = 352 mV; (d) schematic model of the aggregates (dimers) on the surface with staggered configuration.

of the aggregates can clearly be observed with the HBC in the center and 12 surrounding PDI moieties (red boxes), as depicted in the schematic model in Figure 2d. Occasionally, individual structures with the outer ring composed of only six bright spots could be observed, originating from individual molecules (green box). The more frequent occurrence of dimers suggested that even at low concentrations the dyads self-assembled into well-defined aggregates in solution. Depending on the polarity of bias used for the experiments, differences of contrasts between HBC and PDI were observed, indicating that these units behave as isolated species. This was in good agreement with the desired properties, as a nonconjugated ethylene bridge was intentionally introduced

dx.doi.org/10.1021/ja211504a | J. Am. Chem. Soc. 2012, 134, 5876–5886

to prevent ground-state charge-transfer and fast charge recombination after a photoinduced electron transfer. In a next step, the self-organization in solid state was investigated.

Bulk Organization (2D-WAXS, 2D-SAXS). Intermolecular interactions are promoted in the solid state, so the supramolecular organization of dyads **1**−**5** was investigated in bulk by X-ray scattering to gain information about the orientation of the HBC and PDI subunits within the columnar superstructures. As described in the Introduction, the molecular arrangement of the donor−acceptor units within the stacks plays a major role for the charge carrier transport and exciton dissociation. The two-dimensional patterns recorded for **1** in the wide and small-angle range (Figure 3a,b) pointed toward

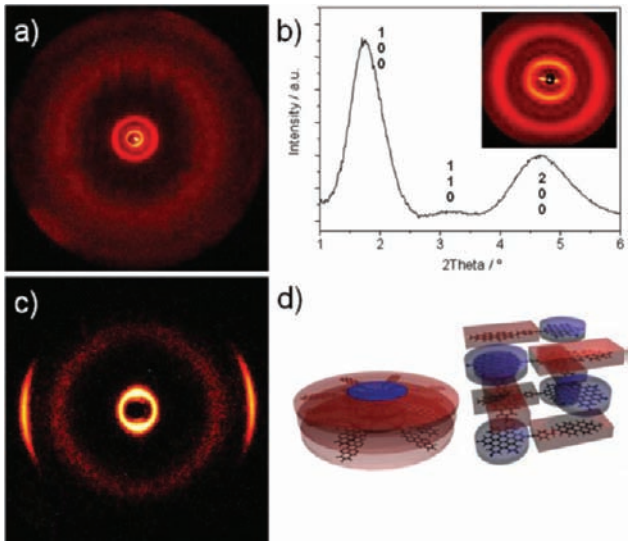

Figure 3. (a) 2D-WAXS and (b) 2D-SAXS (inset) of **1** as powder with the corresponding integration (Miller's indexes are used to assign the reflections), (c) 2D-WAXS of **4** as extruded fiber,[40] (d) Schematic schematic representation of the columnar stacks of star-shaped dyads **1** (left) and **2** and interdigitating stacks of the linear dyad **4** (right).

the formation of columnar stacks that arranged in a hexagonal lattice. The hexagonal intercolumnar distance fitted well with the molecular size of 5.86 nm and indicated that the stacks consisted of individual molecules, as schematically illustrated in Figure 3d. We assume that this type of packing was forced by the local phase separation between the flexible alkyl side chains and the rigid PDI-HBC-PDI cores and the nonstoichiometric ratio between HBC and PDI that did not allow any superstructures with alternating D−A stacking. An identical observation has been made for compound **2**. For both systems, **1** and **2**, no reflections related to intracolumnar order appeared, being characteristic for a so-called disordered columnar structure. This disorder was attributed to the bulky, branched, and long alkyl side chains, which were needed in this case to ensure processability from solution but at the same time decreased the molecular interactions.

Compounds **3** and **4** (Figure 3c) showed a different type of molecular organization. After extrusion into fibers they self-assembled into well-organized discotic stacks with a typical π-stacking distance of 0.34 nm, unlike the above-discussed molecules **1** and **2**. Interestingly, the equatorial positions of the corresponding reflections in the pattern (Figure 3c) suggested that in comparison to other discotics the columnar structures were oriented perpendicular to the alignment direction. This uncommon behavior was related to the high molecular aspect ratio of **3** and **4**. Since no additional reflections appeared in the small-angle scattering region, the small intercolumnar distance determined from the WAXS pattern of only 2.02 nm for **3** and 2.10 nm for **4** implied mixed columns consisting of alternating HBC and PDI subunits. Since **3** and **4** carry the same alkyl side chains and bear the same spacer between the subunits, the intracolumnar distance is identical for both compounds and is independent of the molecular ratio between HBC and PDI. It can be assumed that in the case of **3** the subunits stack in the columns in a more random way due to the higher concentration of PDI, while for the more balanced ratio a strictly alternating arrangement of donor and acceptor units could be found. Recently, the application of solvent vapor diffusion allowed a fine control over the self-assembly of **4** on a surface in thin films, leading to a broad range of different well-defined microstructures with similar alternating arrangements of HBC and PDI.[40]

Optical Characterization. With HBC-6PDI dyads **1** and **2** packing into segregated columnar structures (both in solid state and in solution) and HBC-2PDI **3** as well as HBC-2PDI **4** packing into alternating stacks, the influence of the supramolecular ordering on the inter- and intramolecular energy and charge transfer processes was studied. After selective photoexcitation of the donor HBC a desired photoinduced electron transfer between HBC and PDI would compete with HBC emission, Förster-type resonance energy transfer, and other decay chanels.

UV−vis in Solution. Due to the strong tendency of HBC and PDI to aggregate in the solid state as well as in solution, the absorption and emission spectra often exhibit special features, especially at concentrations typically used for transient fluorescence spectroscopy experiments. Figure 4 shows the

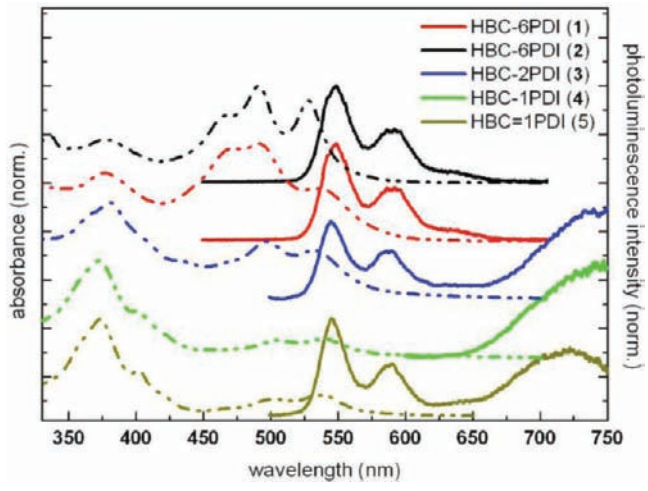

Figure 4. Normalized absorption (dashed lines) and emission spectra (solid lines) of dyads **1**−**5** in toluene, each at a concentration of 10^{-5} mol/L. For photoluminescence measurements HBC moieties were selectively excited at 375 nm with a 100 fs laser pulse.

absorption spectra of the two star-shaped HBC-6PDI dyads molecules **1** and **2** as well as of the linear dyads **3**−**5** in toluene at a concentration of 10^{-5} mol/L, thus at a concentration at which aggregation was likely to occur. Clearly, the absorption spectra were composed of a superposition of the spectrum of the HBC core (325−450 nm) and the PDI chromophores (450−600 nm). Furthermore, the shape of the absorption

dx.doi.org/10.1021/ja211504a | J. Am. Chem. Soc. 2012, 134, 5876−5886

spectra indicated ground-state aggregation of the PDI chromophores in all dyads **1**–**5**, as the absorption differed significantly from that typically seen for single PDI chromophores in diluted solutions.[41] In fact, the reduced intensity of the 0–0 vibronic with respect to the 0–1 vibronic could be interpreted as a clear signature of H-aggregate formation of PDI and was in line with previous reports.[38] However, the extent to which the PDI chromophores aggregated varied between the individual dyads. It is worth mentioning that no additional absorption below the typical optical band gap absorption of HBC and PDI could be observed, which would otherwise have pointed to the presence of ground state CT states.

PL in Solution. After selective photoexcitation of the HBC the emission spectra of the investigated molecules (also shown in Figure 4) dyads **1**–**3** and **5** clearly exhibited the typical vibronic progressions of the fluorescence of PDI chromophores (520–620 nm), while no typical structureless emission spectrum of HBC could be observed between 500 and 600 nm. This exclusive PDI fluorescence detected in the PL measurements indicated a fast and efficient energy transfer from the photoexcited HBC core to the PDI chromophores. This was expected, since the emission spectrum of HBC overlapped well with the absorption of PDI and allowed efficient Förster-type energy transfer. However, compared to the emission of individual PDI molecules in solution, the emission spectra of HBC-6PDI **1** and **2** were significantly broadened and the lower energy vibronic replica of the first electronic transition were more intense than expected and typically observed for individual PDI chromophores. This observation was in line with the interpretation of the absorption spectra, indicating H-aggregate formation. In the present case of the star-shaped HBC-6PDI dyads the PDI emission spectra showed a superposition of the single chromophore emission and a broad and featureless excimer emission, similar to spectra observed previously in related materials.[42] For the linear dyads **3**–**5** an additional emission band between 650–800 nm could be observed in the PL spectra, which was of different origin. This band had previously been assigned to a charge-transfer state emission involving electron transfer between HBC and PDI.[22]

To confirm energy transfer processes after selective photoexcitation of the HBC core in dyads **1**–**3** and **5** and electron transfer processes in dyads **3**–**5**, time-resolved photoluminescence (Figure 5) and absorption measurements (see Supporting Information) were performed. Due to very characteristic lifetimes of the different excited states, this method allowed a clear differentiation between electron and energy transfer processes.

Transient PL/Absorption Spectroscopy in Solution. Photoluminescence decay transients were measured at 560 nm, where isolated individual chromophores (both PDI and HBC) emit and at 700 nm in the red spectral region, where the charge-transfer state recombination emission of the linear dyads **3**–**5** was observed. The kinetics at 560 nm could clearly be assigned to the emission of PDI chromophores with a lifetime of 4.5 ns (described as single-exponential decay), which was well within the range of fluorescence lifetimes typically observed for separated PDI chromophores. The absence of any spectral or decay component from the HBC core for dyads **1**–**5**, which should typically be in the range of 40 ns,[43] suggested that excitons were rapidly transferred from the HBC core by Förster-type fluorescence resonance energy transfer to the PDI chromophores, resulting in solely PDI fluorescence. This was in good agreement with the results of the steady state emission experiments (Figure 4).

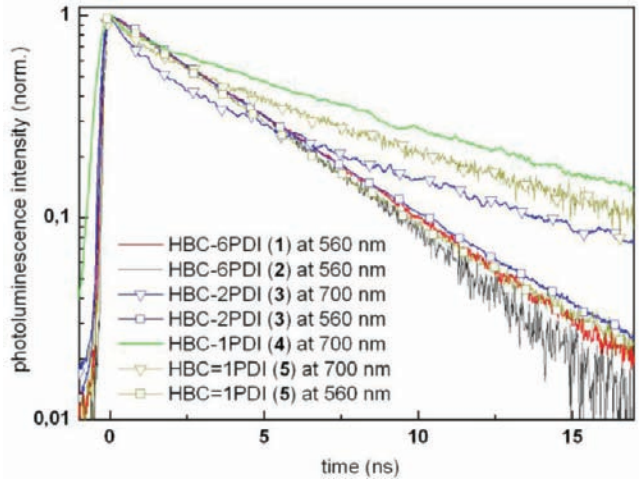

Figure 5. Flourescence decay transients of the dyads **1**–**5** in toluene at a concentration of 10^{-5} mol/L measured by the Streak Camera technique.

For the linear dyads **3**–**5** the lifetime of the emission at 700 nm was determined to be ~10 ns, which was longer than the fluorescence lifetime of separated PDI chromophores but shorter than values typically observed for the PDI excimer emission.[44] To further support the conclusion of a charge-transfer state, we compared transient absorption of both the star-shaped HBC-6PDI **1** and the linear dyad HBC-1PDI **4** in solution (see Supporting Information). The linear dyad showed the characteristic photoinduced absorption peaks of the PDI anion, while the star-shaped molecule did not exhibit any anion-induced peaks, confirming the presence of a charge-transfer state for the linear dyad only. Taking into account our 2D-WAXS measurements, we propose that this emission is related to intermolecular CT-states whose population became possible by the alternating packing motif of HBC and PDI chromophores in these materials.[45] Since the ratio of HBC and PDI in HBC-1PDI **4** was 1:1, a complete conversion of the excitons into intramolecular CT states was possible, and indeed no residual emission from individual PDI chromophores could be observed, while for the linear dyad HBC-2PDI **3**, where the ratio of HBC to PDI was 1:2, concurrent emission from single PDI chromophores and intramolecular HBC-PDI CT states was found. The increased conjugation in the HBC=1PDI dyad **5** in comparison to HBC-1PDI **4** had no significant impact on the photophysical properties of the dyad, except that the ratio of PDI fluorescence and CT state emission differed from those observed for the nonconjugated ethylene bridge.

UV–vis/PL in Drop-Casted Films. We further compared the absorption and photoluminescence measurements of the star-shaped HBC-6PDIs **1** and **2** and the linear dyads **3**–**5** in diluted solution to drop-casted films, to further elucidate if the CT-state formation is an intramolecular process, i.e., charge transfer through the ethylene bridge, or an intermolecular charge-transfer state, originating from the stacking pattern (see Figure 6) and causing interaction between HBC and PDI chromophores on two successive molecules in the stack. This also provides insight into the solid-state photophysics that are more relevant to photovoltaic devices. The absorption bands of the molecules in the solid state were blue-shifted compared to

dx.doi.org/10.1021/ja211504a | J. Am. Chem. Soc. 2012, 134, 5876–5886

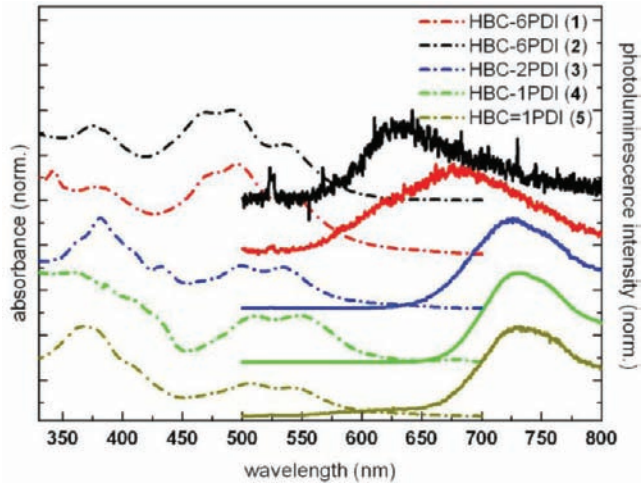

Figure 6. Normalized absorption (dashed lines) and emission spectra (solid lines) of dyads **1**−**5** in drop-casted films, λ_{exc} = 375 nm.

in solution, indicating increased H-aggregation of the PDI chromophores. The solid-state emission bands of the HBC-6PDIs **1** and **2** were also red-shifted compared to solution and found to be broad and featureless. Compared to the CT-emission bands of dyads **3**−**5** observed in solution between 650−800 nm, the emission peaks of HBC-6PDIs **1** and **2** now emerged between 600−700 nm. This emission is typical for the excimer state of aggregated PDI molecules.[44] We observed a further red-shift of the emission of the HBC-6PDI **1** with 10-nonadecyl alkyl chains with respect to HBC-6PDI **2** bearing the 2-decyl-tetradecyl chains. This could be easily understood, since the longer alkyl chains of HBC-6PDI **2** should affect the aggregation of the PDI chromophores. Furthermore, the emission of the linear HBC-PDI dyads **3**−**5** was exclusively dominated by the CT state emission, whereas any isolated PDI chromophore or excimer emission was absent. We noted that similar to the spectra in solution, no emission from the HBC core could be observed here, supporting the notion of fast energy or electron transfer to the PDI.

In sum, we conclude from the time-resolved PL experiments that all excitons generated in the star-shaped HBC-6PDIs **1** and **2** rapidly created an excimer state, which was likely to be a consequence of the interaction between two PDI chromophores. In the linear dyads **3**−**5** the photogenerated excitons underwent a charge transfer process, which was too fast to be resolved in our experiments. However, the nature of the CT-state must have been intermolecular, caused by the alternating donor−acceptor stacking structure, and not by desirable intramolecular electron transfer. The close packing of the molecules led to an overlap of the HBC and PDI π-systems and thus increased the amount of CT-emission. In fact, we could only observe the CT-emission in those dyads **3**−**5** that showed an alternating packing of HBC and PDI, as demonstrated by the morphology experiments. Hence, intermolecular electron transfer was only possible if an alternate packing of HBC and PDI was obtained leading to a reduction of the distance between the chromophores to 0.35 nm, whereas intramolecular charge transfer was impeded by the rigid linker of the dyads, since charges had to overcome a distance of 2.1 nm, possibly with poorer wave function overlap considering the directionality of the π-bonding system. However, intramolecular energy transfer processes from HBC to PDI were observed. These results are consistent with results from kinetic studies on charge transfer in self-organizing D−A dyads, stressing the impact of supramolecular ordering on these processes.[46,47]

Summary and Conclusions. To investigate the intermolecular interactions between covalently linked electron donor−acceptor dyads and their influence on supramolecular organization and fundamental photophysical processes, a series of five HBC-PDI model compounds have been synthesized by Sonogashira coupling reaction. By introducing the ethynyl function to the PDI, multialkynes could be avoided that would otherwise have undergone Glaser-type cross-linking side reactions. This way, even 6-fold substitution toward star-shaped HBC-6PDIs **1** and **2** could be achieved in high yields. Employing rigid linkers, it was possible to control the ratio and the respective distance between donor and acceptor moieties. Dyads **1**−**5** showed a pronounced self-assembly into well-defined superstructures in solution and in the solid state. These aggregates have been extensively studied by STM, 2D-WAXS, and photophysical means to investigate intra- and intermolecular interactions and energy and charge transfer processes. It could be shown that the star-shaped HBC-6PDIs **1** and **2** assembled into columnar structures with nanosegregated stacks of HBC and PDI and a defined intramolecular donor−acceptor distance of 2.1 nm. In contrast to this, the linear dyads HBC-2PDI **3**, HBC-1PDI **4**, and HBC=1PDI **5** formed interdigitating networks with alternating HBC and PDI moieties along the columns, resulting in a defined intermolecular D−A distance of only 0.35 nm and direct π−π interactions.

For dyads **1** and **2**, an efficient Förster-type resonance energy transfer (presumably intramolecular) from the HBC to the PDI was observed, promoted by a high degree of spectral overlap between the HBC emission and the PDI absorption spectra. A photoinduced electron transfer between HBC and PDI, the basic working principle of an organic bulk heterojunction solar cell, did not occur within these aggregates, regardless of whether donor or acceptor were excited. In solution as well as in thin films only emission from PDI chromophores and excimer states could be detected. This indicated that the efficiency of charge transfer was hampered by the distance of more than 1 nm between donor and acceptor and the limited donor−acceptor orbital overlap in the plane of the molecule. However, the linear dyads **3**−**5**, which possessed a direct donor−acceptor overlap between two successive molecules in an aggregate stack, showed CT-emission after HBC excitation in solution. The effect became even more pronounced in the solid state due to enhanced intermolecular interaction compared to in solution. This suggests that intermolecular CT state formation was possible in these systems, but the nanomorphology that enabled this charge transfer was unfortunately unable to provide continuous transport channels for charge carriers as they would be required in electronic devices. The conjugation of the linker in dyads HBC-1PDI **4** and HBC=1PDI **5** had no influence on the photophysical properties, supporting the conclusion that the intermolecular D−A distance was the key factor accelerating the electron transfer. However, the star-shaped HBC-6PDIs **1** and **2** provided potential transport channels for both holes and electrons along the columns. As no electronic interactions between donor and acceptor were found, these independent channels would represent a type of "coaxial cable" that could be used in electronic applications like field-effect transistors. This is currently being investigated in our group.

It could be shown that a careful molecular design is of utmost importance to control the supramolecular organization of

dx.doi.org/10.1021/ja211504a | J. Am. Chem. Soc. 2012, 134, 5876−5886

discotic liquid crystalline materials and by this an effective control over the fundamental photophysical processes like electron and charge transfer and the occurrence of continuous percolation pathways for charges. To promote intramolecular electron transfer, the length of the bridging moiety between HBC and PDI could be reduced or the energy transfer could be impeded by utilizing a different acceptor with less spectral overlap with the HBC emission. With this knowledge, one can now readily develop dyads with targeted properties for a wide variety of potential applications.

EXPERIMENTAL SECTION

***N*-(10-Nonadecyl)-*N*′-(4-iodophenylethyl)-perylene-3,4,9,10-bis(dicarboximide) (8a).** In a single-neck round-bottom flask equipped with a reflux condenser were suspended 860 mg of perylenetetracarboxy dianhydride **6** (2.19 mmol), 1.30 g of 10-aminononadecane (4.58 mmol), and 1.00 g of p-(iodophenyl)-ethylamine[29] **7** (4.58 mmol) in 40 mL of *N*-methyl-2-pyrrolidone (NMP), and the mixture was stirred at 130 °C for 2.5 h under argon atmosphere. Then the solution was neutralized with 2 M HCl, and the product was extracted with dichloromethane (three times) before the organic phase was washed with water and dried over anhydrous magnesium sulfate. After evaporation of the solvent in vacuo the crude product was purified using column chromatography (silica gel, eluent dichloromethane) to yield 661 mg of PDI **8a** as a red solid (34%, 0.74 mmol). EA found: C, 69.2; H, 6.3; N, 3.3. (calcd for $C_{51}H_{55}IN_2O_4$: C, 69.1; H, 6.3; N, 3.2%); ^{1}H NMR (250 MHz, d_2-DCM) δ 8.65 (s, 8H, CH), 7.65 (m, 2H, CH), 7.13 (m, 2H, CH), 5.18 (m, 1H, CH), 4.37 (m, 2H, CH_2), 3.00 (m, 2H, CH_2), 2.20−0.76 (br m, 39H, CH_2 and CH_3); ^{13}C NMR (125 MHz, d_2-TCE, 373 K) δ 163.98, 163.52, 140.24, 138.67, 135.02, 134.77, 132.09, 131.43, 131.38, 129.85, 126.72, 126.67, 124.30, 124.14, 124.06, 92.26, 45.32, 42.31, 37.84, 34.66, 33.02, 31.20, 30.80, 30.77, 30.42, 27.61, 25.98, 25.81, 25.65, 25.49, 25.33, 25.18, 23.66, 14.51; MS (FD, 8 kV) *m*/*z* (%) 886.3 (100) [M$^+$] (calcd for $C_{51}H_{55}IN_2O_4$ 886.3). Mp (°C): thermal decomposition >200 °C.

***N*-(10-Nonadecyl)-*N*′-(4-(triisopropylsilylethinyl)-phenylethyl)-perylene-3,4,9,10-bis(dicarboximide) (9a).** In a dried Schlenk tube were dissolved 705 mg of *N*-(10-nonadecyl)-*N*′-(4-iodophenylethyl)-perylene-3,4,9,10-bis(dicarboximide) (**8a**, 0.795 mmol) and 365 mg of TIPS-acetylene (1.99 mmol) in a solvent mixture of 10 mL of tetrahydrofuran and 2.5 mL of triethylamine, and the solution was degassed with three freeze−vacuum−thaw cycles. Then 22.5 mg of tetrakis(triphenylphosphino)-palladium(0) (32 μmol) and 9.1 mg of copper(I) iodide (48 μmol) were added to the reaction mixture, which was then stirred at 70 °C for 14 h under argon atmosphere. Finally, the reaction solution was poured into methanol, and the precipitate was filtered off and repeatedly washed with methanol. After drying in vacuo the crude product was purified using column chromatography (silica gel, eluent dichloromethane with 1.5% triethylamine) to yield 621 mg of PDI **9a** as a red solid (83%, 0.66 mmol). EA found: C, 78.8; H, 8.1; N, 2.8. (calcd for $C_{62}H_{76}N_2O_4Si$: C, 79.1; H, 8.1; N, 3.0); ^{1}H NMR (250 MHz, d_2-DCM) δ 8.61 (m, 8H, CH), 7.42 (d, *J* = 8.14 Hz, 2H, CH), 7.31 (d, *J* = 8.12 Hz, 2H. CH), 5.18 (m, 1H, CH), 4.39 (m, 2H, CH_2), 3.06 (m, 2H, CH_2), 2.24−1.15 (br m, 33H), 1.13 (m, 21H), 0.82 (br m, 6H, CH_3); ^{13}C NMR (75 MHz, d_2-DCM) δ 162.1, 138.9, 133.5, 133.0, 131.4, 130.1, 128.6, 128.3, 125.2, 125.1, 122.1, 122.1, 121.0, 106.4, 89.5, 40.7, 33.3, 31.7, 31.2, 29.0, 28.7, 26.4, 22.0, 17.8, 13.2, 10.7; MS (FD, 8 kV) *m*/*z* (%) 941.0 (100) [M$^+$] (calcd for $C_{62}H_{76}N_2O_4Si$ 940.6).

***N*-(10-Nonadecyl)-*N*′-(4-ethinylphenylethyl)-perylene-3,4,9,10-bis(dicarboximide) (10a).** In a flask 532 mg of *N*-(10-nonadecyl)-*N*′-(4-(triisopropylsilylethinyl)-phenylethyl)-perylene-3,4,9,10-bis(dicarboximide) (**9a**, 0.565 mmol) was dissolved in 25 mL of tetrahydrofuran, and the solution was degassed with an argon stream for 15 min. Then 1.13 mL of a 1 M solution of tetra-*n*-butylammoniumfluoride (1.13 mmol) in tetrahydrofuran was added, and the solution was stirred at room temperature for 30 min. After evaporation of the solvent in vacuo the crude product was purified using column chromatography (silica gel, eluent dichloromethane) to yield 404 mg of PDI **10a** as a red solid (93%, 0.525 mmol). EA found: C, 80.6; H, 7.1; N, 3.3. (calcd for $C_{53}H_{56}N_2O_4$: C, 81.1; H, 7.2; N, 3.6); ^{1}H NMR (250 MHz, d_2-DCM) δ 8.63 (m, 8H, CH), 7.38 (d, *J* = 8,13 Hz, 2H, CH), 7.25 (d, *J* = 8.16 Hz, 2H, CH), 5.08 (s, 1H, CH), 4.32 (m, 2H, CH_2), 3.03 (s, 1H, acetylene), 2.98 (m, 2H, CH_2), 2.16−1.15 (m, 33H), 0.75 (m, 6H, CH_3); ^{13}C NMR (125 MHz, d_2-DCM) δ 163.33, 140.66, 134.72, 134.23, 132.80, 131.27, 129.78, 129.65, 129.42, 126.44, 126.34, 123.38, 123.28, 120.75, 84.09, 77.39, 55.28, 41.93, 34.55, 32.97, 32.50, 30.21, 29.91, 27.66, 23.26, 18.08, 14.44, 12.95; MS (FD, 8 kV) *m*/*z* (%) 785.6 (100) [M+] (calcd for $C_{53}H_{56}N_2O_4$ 784.4). Mp (°C): 238.

***N*-(2-Decyl-tetradecyl)-*N*′-(4-iodphenylethyl)-perylene-3,4,9,10-bis(dicarboximid) (8b).** In a single-neck round-bottom flask equipped with a reflux condenser were suspended 2.38 g of perylenetetracarboxy dianhydride **6** (6.07 mmol), 4.29 g of 1-amino-2-decyl-tetradecane (12.14 mmol), and 3.00 g of *p*-(iodophenyl)-ethylamine[29] **7** (12.14 mmol) in 100 mL of *N*-methyl-2-pyrrolidone (NMP), and the mixture was stirred at 130 °C for 3 d under argon atmosphere. Then the solution was neutralized with 2 M HCl, and the product was extracted with dichloromethane (three times) before the organic phase was washed with water and dried over anhydrous magnesium sulfate. After evaporation of the solvent in vacuo the crude product was purified using column chromatography (silica gel, eluent dichloromethane) to yield 1.51 g of PDI **8b** as a red solid (26%, 1.57 mmol). EA found: C, 70.3; H, 7.1; N, 3.0. (calcd for $C_{56}H_{55}IN_2O_4$: C, 70.3; H, 6.9; N, 2.9); ^{1}H NMR (500 MHz, d_8-THF) δ 8.16 (s, 8H, CH), 7.68 (d, *J* = 7.9 Hz, 2H, CH), 7.19 (d, *J* = 7.9 Hz, 2H, CH), 4.27 (m, 2H, CH_2), 4.04 (d, *J* = 6.8 Hz, 2H, α-CH_2), 3.03 (m, 2H, CH_2), 1.55−1.20 (m, 41H, CH_2), 0.86 (t, *J* = 6.5 Hz, 6H, CH_3); ^{13}C NMR spectra could not be recorded due to the strong aggregation tendency of the material; MS (FD, 8 kV) *m*/*z* (%) 955.3 (100) [M$^+$] (calcd for $C_{56}H_{55}IN_2O_4$ 956.4). Mp (°C): 235−237.

***N*-(2-Decyl-tetradecyl)-*N*′-(4-(triisopropylsilylethinyl)-phenylethyl)-perylene-3,4,9,10-bis(dicarboximide) (9b).** In a dried Schlenk tube were dissolved 761 of mg *N*-(2-decyl-tetradecyl)-*N*′-(4-iodophenylethyl)-perylene-3,4,9,10-bis(dicarboximide) (**8b**, 0.795 mmol) and 365 mg of TIPS-acetylene (1.99 mmol) in a solvent mixture of 5.5 mL of tetrahydrofuran and 1.4 mL of triethylamine, and the solution was degassed with three freeze−vacuum−thaw cycles. Then 22.5 mg of tetrakis(triphenylphosphino)-palladium(0) (32 μmol) and 9.1 mg of copper(I) iodide (48 μmol) were added to the reaction mixture, which was then stirred at 70 °C for 14 h under argon atmosphere. Finally, the reaction solution was poured into methanol, and the precipitate was filtered off and repeatedly washed with methanol. After drying in vacuo the crude product was purified using column chromatography (silica gel, eluent dichloromethane with 1.5% triethylamine) to yield 583 mg of PDI **9b** as a red solid (73%, 0.576 mmol). EA found: C, 79.4; H, 8.5; N, 2.6. (calcd for $C_{67}H_{86}N_2O_4Si$: C, 79.6; H, 8.6; N, 2.8); ^{1}H NMR (300 MHz, d_2-DCM) δ 8.31 (dd, *J* = 7.8, 7.0 Hz, 4H, CH), 8.31 (d, *J* = 8.1 Hz, 4H, CH), 7.45 (d, *J* = 8.2 Hz, 2H, CH), 7.34 (d, *J* = 8.2 Hz, 2H, CH), 4.32 (m, 2H, CH_2), 4.03 (d, *J* = 7.2 Hz, 2H, α-CH_2), 3.06 (m, 2H, CH_2), 1.48−1.18 (m, 41H, CH_2), 1.14 (br s, 21H, TIPS), 0.86 (m, 6H, CH_3); ^{13}C NMR (75 MHz, d_2-DCM) δ 163.72, 163.30, 140.15, 134.51, 134.17, 132.63, 131.24, 129.53, 123.66, 123.35, 122.17, 41.48, 37.21, 34.57, 32.51, 32.28, 30.63, 30.25, 29.94, 27.06, 23.26, 19.02, 14.44, 11.93; MS (FD, 8 kV) *m*/*z* (%) 1010.8 (100) [M$^+$] (calcd for $C_{67}H_{86}N_2O_4Si$ 1010.6).

***N*-(2-Decyl-tetradecyl)-*N*′-(4-ethinylphenylethyl)-perylene-3,4,9,10-bis(dicarboximide) (10b).** In a flask 560 mg of *N*-(2-decyl-tetradecyl)-*N*′-(4-(triisopropylsilylethinyl)phenylethyl)-perylene-3,4,9,10-bis(dicarboximide) (**9b**, 0.554 mmol) was dissolved in 25 mL of tetrahydrofuran, and the solution was degassed with an argon stream for 15 min. Then 1.2 mL of a 1 M solution of tetra-*n*-butylammoniumfluoride (1.2 mmol) in tetrahydrofuran was added, and the solution was stirred at room temperature for 30 min. After evaporation of the solvent in vacuo the crude product was purified using column chromatography (silica gel, eluent dichloromethane) to yield 460 mg of PDI **10b** as a red solid (97%, 0.538 mmol). EA found: C, 80.9; H, 7.9; N, 3.1. (calcd for $C_{58}H_{66}N_2O_4$: C, 81.5; H, 7.8; N, 3.3); ^{1}H NMR (300 MHz, d_2-DCM) δ 8.18 (dd, *J* = 7.9, 4.9 Hz, 4H,

dx.doi.org/10.1021/ja211504a | *J. Am. Chem. Soc.* 2012, 134, 5876−5886

CH), 7.94 (d, J = 8.1 Hz, 4H, CH), 7.46 (d, J = 8.2 Hz, 2H, CH), 7.35 (d, J = 8.2 Hz, 2H, CH), 4.28 (m, 2H, CH_2), 4.08 (q, J = 7.1 Hz, 1H, β-CH), 3.99 (d, J = 7,1 Hz, 2H, α-CH_2), 3.14 (s, 1H, acetylene), 3.05 (m, 2H, CH_2), 1.50−1.14 (m, 41H), 0.85 (m, 6H, CH_3); ^{13}C NMR (75 MHz, d_2-DCM) δ 163.54, 163.12, 140.66, 134.20, 133.83, 132.81, 131.03, 129.62, 129.11, 125.92, 123.54, 123.18, 123.05, 120.73, 84.09, 78.11, 77.38, 60.80, 45.08, 42.01, 37.25, 34.53, 32.52, 32.28, 30.69, 30.31, 30.27, 29.96, 27.05, 23.26, 21.35, 14.45; MS (FD, 8 kV) m/z (%) 854.0 (100) [M+] (calcd for $C_{58}H_{66}N_2O_4$ 854.5).

***N*-(2-Decyl-tetradecyl)-*N*′-(4-bromopheny)-perylene-3,4,9,10-bis(dicarboximide) (13).** In a single-neck round-bottom flask equipped with a reflux condenser were suspended 100 mg of *N*-(2-decyl-tetradecyl)-3,4,9,10-perylenetetracarboxy-3,4-anhydride-9,10-imide[27] (**12**, 137 μmol) and 118 mg of *p*-bromoaniline (685 μmol) in 5 mL of propanoic acid, and the mixture was stirred at 160 °C for 6 d h under argon atmosphere. Then the solution was neutralized with 2 M HCl, and the product was extracted with dichloromethane (three times) before the organic phase was washed with water and dried over anhydrous magnesium sulfate. After evaporation of the solvent in vacuo the crude product was purified using column chromatography (silica gel, eluent dichloromethane) to yield 65.1 mg of PDI **13** as a red solid (54%, 73.9 μmol). ^{1}H NMR (300 MHz, d_2-TCE) δ 8.48 (d, J = 8.0 Hz, 2H, CH), 8.36 (dd, J = 13.6, 8.1 Hz, 4H, CH), 8.28 (d, J = 8.2 Hz, 2H, CH), 7.65 (d, J = 8.7 Hz, 2H, CH), 7.23 (d, J = 8.6 Hz, 2H, CH), 4.00 (d, J = 7.0 Hz, 2H, α-CH_2), 1.98−0.97 (m, 41H, CH_2), 0.76 (m, 6H, CH_3); ^{13}C NMR (75 MHz, d_2-TCE) δ 163.18, 162.98, 134.61, 133.87, 133.69, 132.46, 131.44, 130.98, 130.48, 129.33, 128.71, 125.94, 125.73, 123.14, 123.01, 122.68, 31.79, 31.54, 29.98, 29.58, 29.54, 29.24, 26.35, 22.59, 14.13; MS (FD, 8 kV) m/z (%) 880.3 (100) [M^+] (calcd for $C_{54}H_{61}BrN_2O_4$ 880.4). Mp (°C): thermal decomposition >300 °C.

***N*-(2-Decyl-tetradecyl)-*N*′-(4-(triisopropylsilylethinyl)-phenyl)-perylene-3,4,9,10-bis(dicarboximide) (14).** In a dried Schlenk tube were dissolved 1.33 g of *N*-(2-decyl-tetradecyl)-*N*′-(4-bromopheny)-perylene-3,4,9,10-bis(dicarboximide) (**13**, 1.51 mmol) and 551 mg of TIPS-acetylene (3.02 mmol) in 25 mL of piperidine, and the solution was degassed with three freeze−vacuum−thaw cycles. Then 87.2 mg of tetrakis(triphenylphosphino)-palladium(0) (75.5 μmol) and 28.8 mg of copper(I) iodide (151 μmol) was added to the reaction mixture, which was then stirred at 70 °C for 14 h under argon atmosphere. Finally, the reaction solution was poured into methanol, and the precipitate was filtered off and repeatedly washed with methanol. After drying in vacuo the crude product was purified using column chromatography (silica gel, eluent dichloromethane with 1.5% triethylamine) to yield 993 mg of PDI **14** as a red solid (67%, 1.01 mmol). ^{1}H NMR (300 MHz, d_2-DCM) δ 8.52 (d, J = 8.0 Hz, 2H, CH), 8.32 (dd, J = 16.3, 8.1 Hz, 4H, CH), 8.22 (d, J = 8.2 Hz, 2H, CH), 7.69 (d, J = 8.5 Hz, 2H, CH), 7.42 (d, J = 8.5 Hz, 2H, CH), 4.05 (d, J = 7.1 Hz, 2H, α-CH_2), 1.62−1.09 (m, 62H, CH_2 and TIPS), 0.76 (m, 6H, CH_3); ^{13}C NMR (75 MHz, d_2-DCM) δ 163.63, 135.99, 134.97, 134.16, 133.31, 131.68, 131.22, 129.53, 126.49, 126.23, 124.71, 124.69, 123.71, 123.62, 123.39, 106.92, 92.55, 44.92, 32.50, 32.29, 30.60, 30.25, 29.94, 29.72, 27.02, 23.26, 19.04, 14.44, 11.93; MS (FD, 8 kV) m/z (%) 981.9 (100) [M^+] (calcd for $C_{65}H_{82}N_2O_4Si$ 982.6). Mp (°C): thermal decomposition >300 °C.

***N*-(2-Decyl-tetradecyl)-*N*′-(4-ethinylphenyl)-perylene-3,4,9,10-bis(dicarboximide) (15).** In a flask 255.7 mg of *N*-(2-decyl-tetradecyl)-*N*′-(4-(triisopropylsilylethinyl)phenyl)-perylene-3,4,9,10-bis(dicarboximide) (**14**, 0.260 mmol) was dissolved in 25 mL of tetrahydrofuran, and the solution was degassed with an argon stream for 15 min. Then 0.6 mL of a 1 M solution of tetra-*n*-butylammoniumfluoride (0.6 mmol) in tetrahydrofuran was added, and the solution was stirred at room temperature for 30 min. After evaporation of the solvent in vacuo the crude product was purified using column chromatography (silica gel, eluent dichloromethane) to yield 212 mg of PDI **15** as a red solid (99%, 0.257 mmol). EA found: C, 81.0; H, 7.7; N, 3.5. (calcd for $C_{56}H_{62}N_2O_4$: C, 81.3; H, 7.6; N, 3.4); ^{1}H NMR (300 MHz, d_8-THF) δ 8.40−8.20 (m, 8H, CH), 7.64 (d, J = 8.4 Hz, 2H, CH), 7.50 (d, J = 8.4 Hz, 2H, CH), 4.06 (m, 2H, α-CH_2), 3.64 (s, 1H, acetylene), 1.97 (m, 1H, β-CH), 1.54−1.19 (m, 41H, -CH_2-), 0.85 (m, 6H, -CH_3); ^{13}C NMR (75 MHz, d_8-THF) δ 163.99, 163.57, 137.46, 135.17, 134.74, 133.35, 131.57, 131.36, 130.55, 130.24, 129.59, 124.46, 124.24, 124.08, 123.62, 37.78, 33.05, 32.94, 31.25, 30.86, 30.82, 30.50, 27.54, 23.73, 14.61; MS (FD, 8 kV) m/z (%) 826.4 (100) [M+] (calcd for $C_{56}H_{62}N_2O_4$ 826.5). Mp (°C): thermal decomposition >300 °C.

Dyad HBC-6PDI with Nonconjugated Linker (1). In a dried Schlenk tube were dissolved 156 mg of *N*-(10-nonadecyl)-*N*′-(4-ethinylphenylethyl)-perylene-3,4,9,10-bis(dicarboximide) (**10a**, 199.2 mmol) and 21.2 mg of hexakis(4-iod)-hexa-*peri*-hexabenzocoronen[32] (**16**, 16.6 μmol) in a solvent mixture of 4.0 mL of piperidine and 1.0 mL of tetrahydrofuran, and the solution was degassed with three freeze−vacuum−thaw cycles. Then 5.7 mg of tetrakis-(triphenylphosphino)-palladium(0) (5.0 μmol) and 1.9 mg of copper(I) iodide (10 μmol) were added to the reaction mixture, which was then stirred at 70 °C for 14 h under argon atmosphere. Finally, the reaction solution was poured into methanol, and the precipitate was filtered off and repeatedly washed with methanol. In a first purification step, the crude product was subjected to Soxhlet extraction with dichloromethane and filtration over a manual preparative GPC column (Bio-Beads S-X1, toluene) in order to separate off insoluble side products. Afterward, recycling preparative GPC was employed to isolate 44.2 mg of dyad **1** in high purity as a red solid (51%, 8.47 μmol). ^{1}H and ^{13}C NMR spectra could not be recorded due to the strong aggregation tendency of the material; MS (MALDI-TOF, TCNQ, solvent-free) m/z (%) 5220.8 (100) [M^+] (calcd for $C_{360}H_{342}N_{12}O_{24}$ 5220.6); UV−vis (tetrahydrofuran, 3.8 × 10^{-6} mol/L) λ_{max}/nm (ε/L/mol·cm) 379 (76827), 471 (125289), 490 (133614); DSC (°C) 14, 41.

Dyad HBC-6PDI with Nonconjugated Linker (2). In a dried Schlenk tube were dissolved 545 mg of *N*-(2-decyl-tetradecyl)-*N*′-(4-ethinylphenylethyl)-perylene-3,4,9,10-bis(dicarboximide) (**10b**, 0.637 mmol) and 67.9 mg of hexakis(4-iodo)-hexa-*peri*-hexabenzocoronene[32] (**16**, 53.1 μmol) in a solvent mixture of 6.0 mL of piperidine and 8.0 mL of tetrahydrofuran, and the solution was degassed with three freeze−vacuum−thaw cycles. Then 18.4 mg of tetrakis-(triphenylphosphino)-palladium(0) (15.9 μmol) and 6.1 mg of copper(I) iodide (31.8 μmol) were added to the reaction mixture, which was then stirred at 80 °C for 14 h under argon atmosphere. Finally, the reaction solution was poured into methanol, and the precipitate was filtered off and repeatedly washed with methanol. In a first purification step, the crude product was subjected to Soxhlet extraction with dichloromethane and filtration over a manual preparative GPC column (Bio-Beads S-X1, toluene) in order to separate off insoluble side products. Afterward, recycling preparative GPC was employed to isolate 92.0 mg of dyad **2** in high purity as a red solid (31%, 16.3 μmol). ^{1}H and ^{13}C NMR spectra could not be recorded due to the strong aggregation tendency of the material; MS (MALDI-TOF, Luftmann, solvent-free, negative modus) m/z (%) 5642.8 (100) [M^+] (calcd for $C_{390}H_{402}N_{12}O_{24}$ 5641.1); DSC (°C) no transitions.

Dyad HBC-2PDI with Nonconjugated Linker (3). In a dried Schlenk tube were dissolved 239 mg of *N*-(2-decyl-tetradecyl)-*N*′-(4-ethinylphenylethyl)-perylene-3,4,9,10-bis(dicarboximide) (**10b**, 0.279 mmol) and 115.7 mg of 1,10-dibromo-4,7,13,16-tetra(3,7-dimethyloctyl)-hexa-*peri*-hexabenzocoronene[34] (**17**, 93 μmol) in a solvent mixture of 7.0 mL of piperidine and 4.0 mL of tetrahydrofuran, and the solution was degassed with three freeze−vacuum−thaw cycles. Then 10.7 mg of tetrakis(triphenylphosphino)-palladium(0) (9.3 μmol) and 1.7 mg of copper(I)iodide (9.3 μmol) was added to the reaction mixture, which was then stirred at 80 °C for 3 d under argon atmosphere. Finally, the reaction solution was poured into methanol, and the precipitate was filtered off and repeatedly washed with methanol. In a first purification step, the crude product was subjected to Soxhlet extraction with dichloromethane and filtration over a manual preparative GPC column (Bio-Beads S-X1, dichloromethane) in order to separate off insoluble side products. As MALDI-TOF MS showed an intense signal for incompletely reacted HBC, the crude product was subjected to another Sonogashira coupling reaction under the same reaction conditions with 2 equiv of PDI **10b**. After 20 h no

more HBC starting material could be detected, and the workup procedure was repeated. Finally, recycling preparative GPC was employed to isolate 25.9 mg of dyad **3** in high purity as a dark red solid (10%, 9.3 μmol). ^{1}H and ^{13}C NMR spectra could not be recorded due to the strong aggregation tendency of the material; MS (MALDI-TOF, dithranol, from tetrahydrofuran solution) m/z (%) 2788.7 (100) [M^+] (calcd for $C_{198}H_{226}N_4O_8$ 2789.8); DSC (°C) no transitions.

Dyad HBC-1PDI with Nonconjugated Linker (4). In a dried Schlenk tube were dissolved 196.8 mg of *N*-(2-decyl-tetradecyl)-*N*′-(4-ethinylphenylethyl)-perylene-3,4,9,10-bis(dicarboximide) (**10b**, 230 μmol) and 165.8 mg of 1-bromo-4,7,10,13,16-penta(3,7-dimethyloctyl)-hexa-*peri*-hexabenzocoronene[34] (**18**, 127 μmol) in a solvent mixture of 5.0 mL of piperidine and 1.0 mL of tetrahydrofuran, and the solution was degassed with three freeze−vacuum−thaw cycles. Then 6.93 mg of tetrakis(triphenylphosphino)-palladium(0) (6.3 μmol) and 2.3 mg of copper(I) iodide (12.7 μmol) were added to the reaction mixture, which was then stirred at 80 °C for 14 h under argon atmosphere. Finally, the reaction solution was poured into methanol, and the precipitate was filtered off and repeatedly washed with methanol. In a first purification step, the crude product was subjected to Soxhlet extraction with dichloromethane and filtration over a manual preparative GPC column (Bio-Beads S-X1, dichloromethane) in order to separate off insoluble side products. Afterward, recycling preparative GPC was employed to isolate 227 mg of dyad **4** in high purity as a dark red solid (86%, 109 μmol). EA found: C, 86.2; H, 8.7; N, 1.1. (calcd for $C_{150}H_{182}N_2O_4$: C, 86.7; H, 8.8; N, 1.4); ^{1}H NMR (500 MHz, d_2-TCE, 393 K) = 8.85−8.46 (m, 12H, CH_{HBC}), 7.70 (d, J = 6.6 Hz, 2H, CH_{phenyl}), 7.53 (d, J = 7.1 Hz, 2H, CH_{phenyl}), 7.27 (m, 4H, CH_{PDI}), 6.57 (m, 4H, CH_{PDI}), 4.50 (s, 2H, $CH_{2bridge}$), 4.02 (s, 2H, α-CH_2), 3.34 (s, 10H, α-CH_2), 3.17 (s, 2H, $CH_{2bridge}$), 2.37−0.90 (m, 136H, CH_2 and CH_3), 0.81 (m, 6H, CH_3); ^{13}C NMR spectra could not be recorded due to the strong aggregation tendency of the material; MS (MALDI-TOF, dithranol, from tetrahydrofuran solution) m/z (%) 2075.8 (100) [M^+] (calcd for $C_{150}H_{182}N_2O_4$ 2076.4); DSC (°C) no transitions.

Dyad HBC=1PDI with Conjugated Linker (5). In a dried Schlenk tube were dissolved 137.8 mg of *N*-(2-decyl-tetradecyl)-*N*′-(4-ethinylphenyl)-perylene-3.4.9.10-bis(dicarboximide) (**15**, 93.3 μmol) and 93.5 mg of 1-bromo-4,7,10,13,16-penta(3,7-dimethyloctyl)-hexa-*peri*-hexabenzocoronene[34] (**18**, 71.8 μmol) in a solvent mixture of 5.0 mL of piperidine and 1.0 mL of tetrahydrofuran, and the solution was degassed with three freeze−vacuum−thaw cycles. Then 4.18 mg of tetrakis(triphenylphosphino)-palladium(0) (3.6 μmol) and 1.3 mg of copper(I)iodide (7.2 μmol) were added to the reaction mixture, which was then stirred at 80 °C for 14 h under argon atmosphere. Finally, the reaction solution was poured into methanol, and the precipitate was filtered off and repeatedly washed with methanol. In a first purification step, the crude product was subjected to Soxhlet extraction with dichloromethane and filtration over a manual preparative GPC column (Bio-Beads S-X1, dichloromethane) in order to separate off insoluble side products. Afterward, five successive recycling preparative GPC steps had to be employed to finally isolate 5.1 mg of dyad **5** in high purity as a dark red solid (5%, 3.6 μmol). ^{1}H NMR (500 MHz, d_2-TCE, 393 K) δ 8.97−8.50 (m, 12H, CH_{HBC}), 8.00 (s, 2H, CH_{phenyl}), 7.69 (s, 2H, CH_{phenyl}), 7.62 (s, 2H, CH_{PDI}), 7.24 (s, 2H, CH_{PDI}), 6.90 (s, 2H, CH_{PDI}), 6.71 (s, 2H, CH_{PDI}), 3.94 (s, 2H, α-CH_2), 3.35 (s, 10H, α-CH_2), 2.98−0.90 (m, 142H, CH_2 and CH_3); ^{13}C NMR spectra could not be recorded due to the strong aggregation tendency of the material; MS (MALDI-TOF, dithranol, from dichloromethane solution) m/z (%) 2048.9 (100) [M^+] (calcd for $C_{148}H_{178}N_2O_4$ 2048.4); DSC (°C) no transitions.

■ ASSOCIATED CONTENT

Supporting Information

Experimental specifications and selected ^{1}H, H−H NOESY, and ^{13}C NMR spectra. This material is available free of charge via the Internet at http://pubs.acs.org.

■ AUTHOR INFORMATION

Corresponding Author

muellen@mpip-mainz.mpg.de

Present Addresses

[†]Evonik Industries AG, Kirschenallee, 64293 Darmstadt, [‡]Germany.

[‡]Molecular and Nanomaterials, University of Leuven, Celestijnenlaan 200f , box 2404, 3001 Heverlee, Belgium.

[§]Department of Chemistry, Graduate School of Science and Engineering, Tokyo Metropolitan University, Hachioji, Tokyo 192-0397.

Notes

The authors declare no competing financial interest.

■ ACKNOWLEDGMENTS

We are grateful to Sreenivasa R. Puniredd for performing X-ray scattering experiments and to Tanya Balandina for supporting the STM imaging. I.A.H. acknowledges a postdoctoral research fellowship of the Alexander von Humboldt Foundation. F.L. thanks the Max Planck Society for funding a Max Planck Research Group. V.K. acknowledges support from the Deutsche Forschungsgemeinschaft (DFG) in the framework of the IRTG 1404.

■ REFERENCES

(1) Cacialli, F.; Wilson, J. S.; Michels, J. J.; Daniel, C.; Silva, C.; Friend, R. H.; Severin, N.; Samorì, P.; Rabe, J. P.; O'Connell, M. J.; Taylor, P. N.; Anderson, H. L. *Nat. Mater.* **2002**, *1*, 160.

(2) Mativetsky, J. M.; Kastler, M.; Savage, R. C.; Gentilini, D.; Palma, M.; Pisula, W.; Müllen, K.; Samorì, P. *Adv. Funct. Mater.* **2009**, *19*, 2486.

(3) Bredas, J.; Calbert, J. P.; da Silva Filho, D.; Cornil, J. *Proc. Natl. Acad. Sci. U.S.A.* **2002**, *99*, 5804.

(4) Pisula, W.; Menon, A.; Stepputat, M.; Lieberwirth, I.; Kolb, U.; Tracz, A.; Sirringhaus, H.; Pakula, T.; Müllen, K. *Adv. Mater.* **2005**, *17*, 684.

(5) Sirringhaus, H. *Adv. Mater.* **2005**, *17*, 2411.

(6) Finlayson, C. E.; Friend, R. H.; Otten, M. B. J.; Schwartz, E.; Cornelissen, J. J. L. M.; Nolte, R. J. M.; Rowan, A. E.; Samorì, P.; Palermo, V.; Liscio, A. *Adv. Funct. Mater.* **2008**, *18*, 3947.

(7) Murphy, A. R.; Frechet, J. M. J. *Chem. Rev.* **2007**, *107*, 1066.

(8) Knipp, D.; Street, R.; Völkel, A.; Ho, J. J. *Appl. Phys.* **2003**, *93*, 347.

(9) Ma, W. L.; Yang, C. Y.; Gong, X.; Lee, K.; Heeger, A. J. *Adv. Funct. Mater.* **2005**, *15*, 1617.

(10) Yang, X. N.; Loos, J.; Veenstra, S. C.; Verhees, W. J. H.; Wienk, M. M.; Kroon, J. M.; Michels, M. A. J.; Janssen, R. A. J. *Nano Lett.* **2005**, *5*, 579.

(11) Yang, X.; Loos, J. *Macromolecules* **2007**, *40*, 1353.

(12) Shaheen, S. E.; Brabec, C. J.; Sariciftci, N. S.; Padinger, F.; Fromherz, T.; Hummelen, J. C. *Appl. Phys. Lett.* **2001**, *78*, 841.

(13) Campoy-Quiles, M.; Ferenczi, T.; Agostinelli, T.; Etchegoin, P. G.; Kim, Y.; Anthopoulos, T. D.; Stavrinou, P. N.; Bradley, D. D. C.; Nelson, J. *Nat. Mater.* **2008**, *7*, 158.

(14) Shin, W.; Jeong, H.; Kim, M.; Jin, S.; Kim, M.; Lee, J.; Lee, J.; Gal, Y. *J. Mater. Chem.* **2006**, *16*, 384.

(15) Schmidt-Mende, L.; Fechtenkötter, A.; Müllen, K.; Moons, E.; Friend, R.; MacKenzie, J. *Science* **2001**, *293*, 1119.

(16) Van de Craats, A.; Warman, J.; Fechtenkötter, A.; Brand, J.; Harbison, M.; Müllen, K. *Adv. Mater.* **1999**, *11*, 1469.

(17) Käfer, D.; Bashir, A.; Dou, X.; Witte, G.; Müllen, K.; Wöll, C. *Adv. Mater.* **2010**, *22*, 384.

(18) Struijk, C. W.; Sieval, A. B.; Dakhorst, J. E. J.; van Dijk, M.; Kimkes, P.; Koehorst, R. B. M.; Donker, H.; Schaafsma, T. J.; Picken, S. J.; van de Craats, A. M. *J. Am. Chem. Soc.* **2000**, *122*, 11057.

(19) Chen, Z.; Debije, M. G.; Debaerdemaeker, T.; Osswald, P.; Würthner, F. *ChemPhysChem* **2004**, *5*, 137.
(20) Würthner, F. *Chem. Commun.* **2004**, 1564.
(21) Langhals, H. *Helv. Chim. Acta* **2005**, *88*, 1309.
(22) Hesse, H. C.; Weickert, J.; Al-Hussein, M.; Dössel, L.; Feng, X.; Müllen, K.; Schmidt-Mende, L. *Sol. Energy Mater. Sol. Cells* **2010**, *94*, 560.
(23) Li, J.; Kastler, M.; Pisula, W.; Robertson, J. W. F.; Wasserfallen, D.; Grimsdale, A. C.; Wu, J.; Müllen, K. *Adv. Funct. Mater.* **2007**, *17*, 2528.
(24) Li, W. S.; Yamamoto, Y.; Fukushima, T.; Saeki, A.; Seki, S.; Tagawa, S.; Masunaga, H.; Sasaki, S.; Takata, M.; Aida, T. *J. Am. Chem. Soc.* **2008**, *130*, 8886.
(25) Wu, J.; Qu, J.; Tchebotareva, N.; Müllen, K. *Tetrahedron Lett.* **2005**, *46*, 1565.
(26) Samorì, P.; Fechtenkötter, A.; Reuther, E.; Watson, M. D.; Severin, N.; Müllen, K.; Rabe, J. P. *Adv. Mater.* **2006**, *18*, 1317.
(27) Xue, C.; Sun, R.; Annab, R.; Abadi, D.; Jin, S. *Tetrahedron Lett.* **2009**, *50*, 853.
(28) Odom, S.; Kelley, R.; Ohira, S.; Ensley, T.; Huang, C.; Padilha, L.; Webster, S.; Coropceanu, V.; Barlow, S.; Hagan, D. *J. Phys. Chem. A* **2009**, *113*, 10826.
(29) Wyffels, L.; Muccioli, G.; De Bruyne, S.; Moerman, L.; Sambre, J.; Lambert, D.; De Vos, F. *J. Med. Chem.* **2009**, *52*, 4613.
(30) Kozma, E.; Munno, F.; Kotowski, D.; Bertini, F.; Luzzati, S.; Catellani, M. *Synth. Met.* **2010**, *160*, 996.
(31) Guo, X.; Watson, M. *Org. Lett.* **2008**, *10*, 5333.
(32) Wu, J.; Baumgarten, M.; Debije, M.; Warman, J.; Müllen, K. *Angew. Chem., Int. Ed.* **2004**, *43*, 5331.
(33) Simpson, C. D.; Brand, J. D.; Berresheim, A. J.; Przybilla, L.; Räder, H. J.; Müllen, K. *Chem.—Eur. J.* **2002**, *8*, 1424.
(34) Fechtenkötter, A.; Tchebotareva, N.; Watson, M.; Müllen, K. *Tetrahedron* **2001**, *57*, 3769.
(35) Trimpin, S.; Rouhanipour, A.; Az, R.; Räder, H. J.; Müllen, K. *Rapid Commun. Mass Spectrom.* **2001**, *15*, 1364.
(36) Trimpin, S.; Keune, S.; Räder, H.; Müllen, K. *J. Am. Soc. Mass. Spectrom.* **2006**, *17*, 661.
(37) Watson, M. D.; Jäckel, F.; Severin, N.; Rabe, J. P.; Müllen, K. *J. Am. Chem. Soc.* **2004**, *126*, 1402.
(38) Würthner, F.; Thalacker, C.; Diele, S.; Tschierske, C. *Chem.—Eur. J.* **2001**, *7*, 2245.
(39) Kasha, M. *Radiat. Res.* **1963**, *20*, 55.
(40) Wang, S.; Dössel, L.; Mavrinskiy, A.; Gao, P.; Feng, X.; Pisula, W.; Müllen, K. *Small* **2011**, *7*, 2840.
(41) Kamm, V.; Battagliarin, G.; Howard, I. A.; Pisula, W.; Mavrinskiy, A.; Li, C.; Müllen, K.; Laquai, F. *Adv. Energy Mater* **2011**, *1*, 297.
(42) Albert Seifried, S.; Finlayson, C. E.; Laquai, F.; Friend, R. H.; Swager, T. M.; Kouwer, P. H. J.; Jurí ek, M.; Kitto, H. J.; Valster, S.; Nolte, R. J. M. *Chem.—Eur. J.* **2010**, *16*, 10021.
(43) Kim, K. Y.; Liu, S.; Köse, M. E.; Schanze, K. S. *Inorg. Chem.* **2006**, *45*, 2509.
(44) Keivanidis, P. E.; Howard, I. A.; Friend, R. H. *Adv. Funct. Mater.* **2008**, *18*, 3189.
(45) Kircher, T.; Löhmannsröben, H. G. *Phys. Chem. Chem. Phys.* **1999**, *1*, 3987.
(46) Beckers, E. H. A.; Meskers, S. C. J.; Schenning, A. P. H. J.; Chen, Z.; Würthner, F.; Marsal, P.; Beljonne, D.; Cornil, J.; Janssen, R. A. J. *J. Am. Chem. Soc.* **2006**, *128*, 649.
(47) Isosomppi, M.; Tkachenko, N. V.; Efimov, A.; Vahasalo, H.; Jukola, J.; Vainiotalo, P.; Lemmetyinen, H. *Chem. Phys. Lett.* **2006**, *430*, 36.